

Research Paper

CD137 promotes bone metastasis of breast cancer by enhancing the migration and osteoclast differentiation of monocytes/macrophages

Pengling Jiang^{1,3,4}, Wenjuan Gao², Tiansi Ma², Rongrong Wang², Yongjun Piao², Xiaoli Dong², Peng Wang², Xuehui Zhang^{3,5}, Yanhua Liu^{2,6}, Weijun Su^{2,6}, Rong Xiang^{2,6}, Jin Zhang^{1,3,4}✉, Na Li^{2,6}✉

1. Third Department of Breast Cancer, Tianjin Medical University Cancer Institute and Hospital, National Clinical Research Center for Cancer, Key Laboratory of Cancer Prevention and Therapy, Tianjin, China;
2. School of Medicine, Nankai University, 94 Weijin Road, Tianjin, China;
3. Tianjin's Clinical Research Center for Cancer, Tianjin, China;
4. Key Laboratory of Breast Cancer Prevention and Therapy, Tianjin Medical University, Ministry of Education, Tianjin, China;
5. Department of Blood Transfusion, Tianjin Medical University Cancer Institute and Hospital, National Clinical Research Center for Cancer, Key Laboratory of Cancer Prevention and Therapy, Tianjin, China;
6. Tianjin Key Laboratory of Tumour Microenvironment and Neurovascular Regulation, Tianjin, China.

✉ Corresponding authors: Dr. Jin Zhang, zhangjin@tjmuch.com; Dr. Na Li, lina08@nankai.edu.cn.

© Ivyspring International Publisher. This is an open access article distributed under the terms of the Creative Commons Attribution (CC BY-NC) license (<https://creativecommons.org/licenses/by-nc/4.0/>). See <http://ivyspring.com/terms> for full terms and conditions.

Received: 2018.08.31; Accepted: 2019.03.25; Published: 2019.05.09

Abstract

Rationale: Bone is one of the most common metastatic sites of breast cancer. CD137 (4-1BB), a member of the tumor necrosis factor (TNF) receptor superfamily, is mainly expressed in activated leukocytes. Previous study demonstrates the effect of CD137-CD137L bidirectional signaling pathway on RANKL-mediated osteoclastogenesis. However, the role of CD137 in bone metastasis of breast cancer needs further study.

Methods: Stable monocyte/macrophage cell lines with *Cd137* overexpression and silencing were established. Western blot, real-time PCR, transwell and tartrate-resistant acid phosphatase staining were used to detect the regulatory effect of CD137 on migration and osteoclastogenesis of monocytes/macrophages *in vitro*. Spontaneous bone metastasis mouse model was established, bioluminescent images, immunohistochemistry and histology assay were performed to detect the function of CD137 in bone metastasis *in vivo*.

Results: We found that CD137 promotes the migration of monocytes/macrophages to tumor microenvironment by upregulating the expression of Fra1. It also promoted the differentiation of monocytes/macrophages into osteoclasts at the same time, thus providing a favorable microenvironment for the colonization and growth of breast cancer cells in bone. Based on these findings, a novel F4/80-targeted liposomal nanoparticle encapsulating the anti-CD137 blocking antibody (NP- α CD137 Ab-F4/80) was synthesized. This nanoparticle could inhibit both bone and lung metastases of 4T1 breast cancer cells with high efficacy *in vivo*. In addition, it increased the therapeutic efficacy of Fra1 inhibitor on tumor metastasis.

Conclusions: Taken together, these findings reveal the promotion effect of macrophage/monocyte CD137 on bone metastases and provide a promising therapeutic strategy for metastasis of breast cancer.

Key words: liposomal nanoparticles, anti-CD137 antibody, Fra1, breast cancer, bone metastasis, metastatic niche.

Introduction

Breast cancer is one of the most common malignancies in women and is among the leading causes of cancer death for female in the United States

[1]. Bone is one of the most common sites of breast cancer metastases, since about 80% of patients with metastatic breast cancer develop bone metastases [2].

Regarding the molecular mechanisms of bone metastases in breast cancer, a "seed-soil" theory of tumor metastases was proposed and gained the identity [3, 4]. This theory suggests that the expression of specific cytokines in the local microenvironment increases the chemotactic and adhesive ability of the tumor cells greatly, thus promotes the formation of metastases. It highlights the interaction between tumor cells and the targeted organ microenvironment and explains the organ selectivity of tumor bone metastases. The molecular mechanisms of bone metastases of breast cancer still need to be further explored. Therefore, in-depth study of the underlying mechanisms and looking for effective therapeutic targets are particularly important.

CD137 (4-1BB), a member of the tumor necrosis factor (TNF) receptor superfamily, is mainly expressed in activated leukocytes, including T cells, B cells, eosinophils, monocytes and natural killer (NK) cells [5]. As a ligand of CD137, CD137L belongs to the TNF ligand family and is expressed in antigen-presenting cells [6, 7]. It is also expressed in various types of tumor cells [8, 9]. CD137 was found to activate and increase the adherence of monocytes [10, 11]. Studies have found that CD137 and CD137L coexist in different parts of the tumor tissue [12]. These findings suggest a possible interaction between tumor cells and macrophages in tumor microenvironment through the CD137L-CD137 signaling pathway. Previous studies found that CD137 and RANK share common downstream signaling pathways, and CD137-CD137L bidirectional signaling pathway affect RANKL-mediated osteoclastogenesis [13, 14]. However, it remains unclear whether CD137 is involved in bone metastases of breast cancer.

In 1997, Melero et al. discovered that agonist anti-CD137 monoclonal antibodies (mAbs) can effectively reduce tumor volume in mice [15]. Agonist anti-CD137 mAb exerts anti-tumor effects by promoting cell survival and enhancing the activity of cytotoxic T cells [15, 16]. In recent years, CD137 agonists, such as Utomilumab (PF-05082566) and Urelumab have undergone clinical trials for pancreatic cancer, melanoma, lung cancer and kidney cancer, etc. [17, 18]. However, to our knowledge, the usage of CD137 as a therapeutic target for breast cancer metastases has not been reported yet.

Macrophages, as a component of tumor microenvironment, play important roles in tumor progression [19-21]. The monocytes can differentiate into macrophages and osteoclasts in bone microenvironment and participate in the remodeling, repairing and regulating the homeostasis of bone [19, 22]. Previous studies found that macrophages

promote bone metastases of tumors. For example, colony stimulating factor 1 (CSF-1) and colony stimulating factor 1 receptor (CSF-1R) are involved in the infiltration of monocytes/macrophages in tumors [23, 24]. CSF-1 potentiates bone metastases of lung cancer [25]. In addition, several studies found that CCL2 increases bone metastases of prostate cancer by promoting the recruitment of macrophages and osteoclasts [26]. Depletion of monocytes/macrophages or reducing the infiltration of macrophages in the bone microenvironment effectively inhibits the occurrence of bone metastasis [19, 27]. These findings provide a new idea for the treatment of bone metastasis of breast cancer by targeting macrophages.

There are specific and established markers on the membrane of monocytes/macrophages, such as F4/80, CD68, CD163, etc. [28-30]. Currently, studies that using these membrane receptors to target macrophages are reported. For example, legumain was used as a target for the depletion of macrophages and against breast cancer [31]. CD163 was exploited as a target for delivery of drugs to monocytes by using stealth liposomes [32]. Nanoparticles (NPs) have been widely used for the delivery of agents to target sites [33]. The advantage of NPs delivery systems is their ability to deliver agents efficiently to target cells in their bioavailable forms [34]. For example, CD44-targeted NPs can specifically deliver antibodies to tumor sites specially, thereby exerting the therapeutic effect on tumor [35]. This delivery method can reduce the side-effect of agents, thereby improve their therapeutic efficacy.

Here, we found that CD137 can regulate the migration of monocytes/macrophages to tumor microenvironment both *in vitro* and *in vivo*. Moreover, CD137 promoted the differentiation of monocytes/macrophages into osteoclasts to form a microenvironment suitable for the colonization of tumor cells, which ultimately enhanced bone metastases of breast cancer. According to this finding, a novel F4/80-targeted liposomal nanoparticle encapsulating the anti-CD137 blocking antibody was designed. We found this monocyte/macrophage targeted NP shows high efficacy in inhibiting the bone metastases of breast cancer. This study provides a promising strategy for the treatment of bone metastasis of breast cancer.

Methods

Ethics statement and patients' sample

All animal experiments were carried out according to guidelines for the use and care of laboratory animals approved by the Research Institute

Ethics Committee of Nankai University. The serum was collected from normal female and breast cancer female patients with histological evidence who were admitted to the Chinese PLA General Hospital and Tianjin Medical University Cancer Institute and Hospital in 2015 and 2016. All patients signed the informed contents. The patients were in the state of initial diagnosis, follow-up or recurrence. The serum samples were collected within 2 hours of venous blood sampling and stored at -80°C . The study was approved by the ethics committee of Chinese PLA General Hospital and Tianjin Medical University Cancer Institute and Hospital.

TCGA data analysis

The Cancer Genome Atlas (TCGA) breast cancer dataset was obtained from UCSC Xena browser (<http://xena.ucsc.edu/>). The raw expression counts of 1,196 individual primary human breast cancer tissues were used for the analysis.

Determination of serum sCD68 protein levels

The concentration of serum sCD68 was determined by using the CD68 enzyme-linked immunosorbent assay (ELISA) Kit (antibodies-online, Shanghai, China). The ELISA was performed according to the manufacturer's instructions. The absorbance was measured in a microplate reader at 450 nm (OD450, Thermo Fisher Scientific, Waltham, MA, USA).

Cell culture

RAW264.7 and 4T1 cell lines were obtained from Dr. Ralph A. Reisfeld (The Scripps Research Institute, CA, USA). RAW264.7 and 4T1 cells were cultured in the RPMI 1640 medium supplemented with 10% FBS, 100 U/mL penicillin and 0.1 mg/mL streptomycin. Stable 4T1 cell line with overexpression of firefly luciferase (4T1FL) was established following the procedure described before [36]. RAW264.7 cells were transfected with lentivirus carrying the pLV-EF1 α -Renilla luciferase-Bsd plasmid and selected by adding blasticidin to the culture medium to establish the stable polyclonal RAW264.7 cell line with renilla luciferase (RL) overexpression (RawRL).

cDNA of mus *Cd137* and shRNAs targeting mus *Cd137* were cloned into the pLV-EF1 α -MCS-IRES-puro and pLV-H1-EF1 α -puro plasmids, respectively (Biosettia Inc., San Diego, CA, USA). The sequences of shRNAs were: sh1-CD137: GGAGTGTGAGTGCATTGAAGG; sh2-CD137: GGTCATTGTGCTGCTGCTAGT. RawRL cells were infected with lentivirus carrying above plasmids, pLV-EF1 α -MCS-IRES-puro and pLV-H1-EF1 α -puro plasmids carrying scramble shRNA (SC), respectively

and selected by adding puromycin to the cell culture medium to obtain stable polyclonal cell lines with *Cd137* overexpression (RawRL-CD137) and silencing (RawRL-shCD137), and their corresponding controls (RawRL-Con, RawRL-SC), respectively.

cDNA of mus *Fra1* was cloned into the pLV-EF1 α -MCS-IRES-puro plasmid (Biosettia Inc., San Diego, CA, USA). RAW264.7 and RawRL-shCD137 cells were transiently transfected with lentivirus carrying pLV-EF1 α -Fra1-IRES-puro or the empty plasmids to obtain the cell lines with *Fra1* overexpression (Raw-Fra1, RawRL-shCD137-Fra1) and the controls (Raw-Con, RawRL-shCD137-Con), respectively.

Western blotting

Cell lysates were prepared as previously described [37]. 30 μg protein lysate, 50 μL human serums, or 40 μL cell supernatant was loaded on a 12% Bis-Tris gel and transferred onto a PVDF membrane. The blots were detected by using the following primary antibodies: anti- β -actin, Fra1, p-Fra1 (Ser265) (Cell Signaling Technology, Danvers, MA, USA), anti-Renilla luciferase (Affinity Biosciences, Cincinnati, OH, USA), anti-CD137 (abcam, Cambridge, UK), anti-hCD137L (R&D Systems Inc., Minneapolis, MN, USA), anti-mCD137L (Bioss Antibodies, Beijing, China) antibodies. These primary antibodies were detected with proper secondary antibodies. Proteins were detected by ECL detection reagent (Millipore, Billerica, MA, USA).

The densitometry of the blot was obtained by using the Image J software (National Institutes of Health, USA) and was compared with that of β -actin for each sample to obtain the normalized value. The normalized value of each blot was compared to that of its control to obtain the relative fold change (RFC), at least 2 independent experiments were performed. The mean RFC value of each blot was indicated at the bottom. The normalized protein expression level of serum sCD137 from healthy and breast cancer patients was compared with that of one healthy control people to obtain the RFC.

Transwell assay

Cell migration assay of RAW264.7 and primarily cultured macrophages ($\text{M}\Phi$) was evaluated by using a 5- μm pore size transwell chamber (Millipore, Billerica, MA, USA). 1×10^5 RAW264.7 cells or $\text{M}\Phi$ were placed into each upper chamber of 24-well transwell containing 1% FBS medium. The lower chamber was filled with 500 μL supernatant of 4T1FL or plated with 4T1FL cells that were cultured in 500 μL culture medium. After 24 hours of migration, the cells in the upper chamber were removed and cleaned by a

cotton swab. The cells that penetrated and attached to the bottom of the chamber membrane were stained by 1 % crystal violet and subjected to microscope image under a 10× objective. The cell number per image field was averaged from 3 different image fields for each transwell assay; at least three independent experiments were performed.

To test migration-regulation effect of different agents, IgG, monoclonal anti-CD137 blocking antibody (clone 6D295, Santa Cruz Biotechnology, Inc., Dallas, TX, USA) or monoclonal anti-CD137 ligand (L) blocking antibody (clone TKS-1, Sungene Biotech, Tianjin, China) was added to the lower chamber to reach the final concentration of 10 µg/mL, Fra1 inhibitor-SKLB816 kindly provided by Dr. Shengyong Yang (State Key Laboratory of Biotherapy and Cancer Center, Sichuan University, Chengdu, China) was added to the lower chamber to reach the final concentration of 0.5 µM.

Wound-healing assay

RawRL cells were plated in a 24-well plate. When they grew to 100% confluence, a 'wound' was made in the middle of the well by using a 10 µL pipette tip, the concentration of FBS of culture medium was changed from 10% to 1% at the same time. The wound-healing process was recorded at 0 hour and 24 hours after the scratch under an objective. The wound healing rate (%) = the distance of wound recovered/ the distance of the original wound × 100%.

RNA-seq

The RawRL-CD137 and the RawRL-Con cells were harvested. 4 µg total RNA from each sample was extracted by using TRIzol reagent. The transcriptome data of both cell lines were profiled and compared by using a BGISEQ-500 (Beijing Genomics Institute at Shenzhen, China). The RNA-seq was performed three times. Those migration-associated genes with consistent false discovery rate (FDR) < 0.001 and Log₂ CD137/Con > 0.5 or < -0.5 were selected out as the targets of CD137. RNA-Seq data have been deposited to NCBI Gene Expression Omnibus (GEO) database (GSE130013).

Osteoclast differentiation and TRAP staining

RawRL cells were plated at a density of 2×10⁴ cells per well in a 24-well culture plate and differentiated with 10 ng/mL M-CSF and 100 ng/mL RANKL (R&D Systems Inc., Minneapolis, MN, USA) for 9 days. Culture medium was replaced every 48 hours. Then cells were washed, fixed and stained for tartrate-resistant acid phosphatase (TRAP, Sigma-Aldrich, St Louis, MO, USA) according to the manufacturer's instructions. The TRAP⁺ cell number

per image field was averaged from 3 different image fields for each well, three independent experiments were performed.

For analysis of the parameters of osteoclasts in the bone metastatic lesions, 7-µm sections were stained with hematoxylin and TRAP, respectively.

Real-time PCR analysis

Total RNAs were isolated with TRIzol™ reagent (Thermo Fisher Scientific, Waltham, MA, USA) and reversely transcribed into cDNAs as described before [36]. A Hieff™ qPCR SYBR® Green Master Mix (YEASEN Biotechnology, Shanghai, China) was used. The mRNA expression of osteoclast-associated genes including *Dcstamp*, *Atp6v0d2*, *Itgb3*, *Ctsk*, *Opg*, *RANKL* and *TRAP* was detected; the expression of *Gapdh* was used as the loading control. 2^{-ΔΔCt} method was used to determine relative fold changes for the expression of mRNAs. Assays were performed in triplicate. The primer sequences were shown in **Table S1**; the primer sequences for *Gapdh* were described before [38].

Histology and immunohistochemistry staining

Immunostaining was performed on human breast tissue array (Alenabio Co., Xi'an, China) and mouse tissues. All mouse tissues were fixed in 4% paraformaldehyde for 24 hours. Bones were decalcified in 10% EDTA for 7 days at 4°C. Standard immunostaining techniques were used to prepare the sections for histology and immunohistochemistry staining. CD137, CD137L, Renilla luciferase, Ki67, and F4/80 were stained by using the following primary antibodies: anti-CD137 (abcam, Cambridge, UK), anti-CD137L (R&D Systems Inc., Minneapolis, MN, USA), anti-Renilla luciferase (Affinity Biosciences, Cincinnati, OH, USA), anti-Ki67 and F4/80 (abcam, Cambridge, UK) antibodies. The streptavidin-biotin detection system was applied and 3, 3'-diaminobenzidine (DAB) was used. The images were recorded by using Olympus BX51 fluorescent microscopy (Olympus, Tokyo, Japan).

Preparation of liposomal nanoparticles (NPs)

Liposomal nanoparticles were prepared as previously described [35]. The lipid mixture was composed of DOPE, DOPC and cholesterol (1:1:1 molar ratio).

For preparation of per 1 mL of the liposomal nanoparticles or F4/80 targeted liposomal nanoparticles encapsulating monoclonal anti-CD137 or PE conjugated anti-CD137 antibody (NPs-αCD137 Ab-F4/80 or NPs-αCD137 Ab-PE-F4/80), 30 µg anti-CD137 blocking antibody (clone 6D295, Santa Cruz Biotechnology, Inc., Dallas, TX, USA) or anti-CD137 Ab-PE (BD Biosciences, San Jose, CA,

USA) was dissolved in 1 mL PBS (pH7.4) at 4°C for 15 min, then mixed with 1 mL lipid films at 4°C for 1 hour. After fully hydration, the liposomes were extruded 10 times through 100 nm polycarbonate membrane filter. After encapsulation, the free antibody was removed by size exclusion chromatography system (GE Healthcare, Chicago, IL, USA). The F4/80 targeted liposomes were prepared following the method described before [35]. Briefly, monoclonal anti-F4/80 antibody was conjugated with DSPE-PEG3400-NHS at a 1:10 molar ratio. Then, liposomes were mixed with anti-F4/80 Ab-PEG conjugates at a molar ratio of 100:1 for 4-8 hours with continuous stirring.

GloMax®-Multi Detection System (Promega, Madison, WI, USA) was used to measure the encapsulation efficiency for NPs. The Mass (M) of free antibody (Ab) presented in the supernatant was determined by the fluorescence intensity value excited at 490 nm and at the emission wavelength of 510-570 nm, then was calculated based on the calibration curve. Encapsulation efficiency(%)=M (feeding Ab) – M(Ab in supernatant)/M (feeding Ab)×100% [35].

Allograft tumor model and the treatment

All animal studies were performed according to the guidelines of Nankai University Animal Care and Use Committee. Female BALB/c mice aged 6-8 weeks were used in all animal studies. Bone metastases were measured by BLI, necropsy and/or hematoxylin and eosin (H&E) staining on bone paraffin sections.

To determine the effect of monocyte/macrophage CD137 on breast cancer metastases, 1×10^5 4T1FL cells and 1×10^4 RawRL cells were subcutaneously co-injected around the fourth mammary gland of each mouse. After 14 days of inoculation, the tumors were surgically removed. Development of metastases was monitored by bioluminescent images (BLI) with the IVIS Spectrum In Vivo System (PerkinElmer). BLI signal data were acquired by subtracting the background and analyzed using Living Image Software (PerkinElmer). The mice were sacrificed 4 weeks after the surgical resection, forelimb and hindlimb bones, spines, ribs and lungs were harvested from each group.

1×10^5 4T1FL cells were injected around the fourth mammary gland of each mouse subcutaneously to establish a 4T1FL-allograft mouse model in the following four experiments:

To determine the effect of clodronate liposome on metastases, after 1 week of tumor-inoculation, we administered clodronate liposome (YEASEN Biotechnology, Shanghai, China) intraperitoneally at a dose of 1 mg/20g body weight (BW) for five times.

To determine the therapeutic effect of NPs- α CD137 Ab-F4/80 on metastases, the 4T1FL-allograft mice were randomly separated into five groups and injected with PBS, α CD137 Ab, NPs-IgG-F4/80, NPs- α CD137 Ab or NPs- α CD137 Ab-F4/80 (200 μ L/20g BW of PBS or NPs each time, 6 μ g /20g BW of Ab each time) through the tail vein, respectively.

In the combined therapy experiments, the 4T1FL-allograft mice were randomly separated into four groups and injected with PBS, NPs- α CD137 Ab-F4/80, SKLB816, NPs- α CD137 Ab-F4/80 plus SKLB816 (200 μ L/20g BW of PBS or NPs each time, 1.184 μ g /20g BW of SKLB816 each time) through the tail vein, respectively.

To analyze of the bio-distribution of antibody in tumor-bearing mice treated with F4/80 targeted NPs, the 4T1FL-allograft mice were randomly separated into two groups. 1 week after the inoculation, NPs- α CD137 Ab-PE or NPs- α CD137 Ab-PE-F4/80 (6 μ g Ab/20g BW) were injected to the mice via tail vein separately. The mice were sacrificed 6 hours after the injection. Primary tumor tissues were removed and subjected to immunofluorescent staining and bio-distribution assay of the NPs following the procedure described before [35].

Quantification of lung metastatic foci number and areas

After the lung sections were stained with H&E, the number of lung metastatic foci was recorded under a 4 \times objective, and the area of lung metastases and the total area of lung lobes were calculated by using photoshop software (Adobe). Lung metastatic area ratio (%) =lung metastatic area / total five lung lobes area×100%.

Immunofluorescent staining

The frozen tissue sections were fixed in 4% paraformaldehyde for 15 minutes and then incubated with anti-CD68 (Proteintech, Wuhan, China), anti-CD3 Ab-FITC (Thermo Fisher Scientific, Waltham, MA, USA), anti-CD69 (Bioss Antibodies, Beijing, China), anti-Ki67 (abcam, Cambridge, UK) antibodies overnight at 4 °C, the un-conjugated primary antibodies were further incubated with Alexa Fluor 488 or Alexa Fluor 594 conjugated secondary antibody (Molecular Probes, Eugene, OR, USA) at room temperature for 1 hour. They were finally counterstained with DAPI (4',6-diamidino-2-phenylindole, Sigma-Aldrich, St. Louis, MO, USA). Images were acquired by using a laser scanning confocal microscope (Olympus, Tokyo, Japan).

Isolation of mouse peritoneal cavity macrophages and primary cell culture

1 mL thioglycollate solution (thioglycollate (Sigma-Aldrich) dissolved in PBS to the final concentration of 4%) was injected intraperitoneally to female BALB/c mice at 6~8 weeks old. After 4 days, the mice were subjected to peritoneal lavage treatment by using ice cold RPMI 1640 supplemented with 10% FBS. The irrigation fluid was collected and then centrifuged at 1,500 rpm for 5 min. The pellet containing the peritoneal macrophages was collected and cultured in RPMI 1640 supplemented with 10% FBS. Six hours after plating, the macrophages attached to the bottom of culture dishes, red blood cells were removed by gently blowing and changing of culture medium.

Cell treatment

IgG, monoclonal anti-CD137 blocking antibody (clone 6D295, Santa Cruz Biotechnology, Inc., Dallas, TX, USA) were added to the culture medium of 4T1FL. RawRL-CD137 and M Φ to reach the final concentration of 10 μ g/mL, respectively. SKLB816 was added to the culture medium of RawRL-CD137 and 4T1FL cells to reach the final concentration of 0.5 μ M. The cells were treated for 48 hours and then collected and subjected to Western blot. Cell viability were tested by using CCK8 kit (Dojindo, Shanghai, China) following the manufacturer's instructions and measured as absorbance at 450nm.

Fluorescence-activated cell sorting (FACS) analysis

7×10^5 4T1FL cells were subcutaneously injected to the fourth mammary gland of each female BALB/c mouse aged 6-8 weeks. 8 days after the inoculation, PBS (200 μ L/20g BW) or NPs- α CD137 Ab-F4/80 (6 μ g Ab/20g BW) was injected to the mice via tail vein separately. The mice were sacrificed 24 hours after the injection. The spleen of each mouse was removed and grinded, red blood cells were removed by using Red Blood Cell Lysis Solution (SolarBio, Beijing, China) according to manufacturer's instructions. The spleen leukocytes were re-suspended in PBS and then separated into two tubes: one tube was incubated with anti-CD3 Ab-PE-Cy7 (Sungene Biotech, Tianjin, China), anti-CD69 Ab-APC, anti-CD8 Ab-PerCP-Cy5.5 (Thermo Fisher Scientific, Waltham, MA, USA), anti-CD4 Ab-PE and anti-CD44 Ab-FITC (BD Biosciences, San Jose, CA, USA), another tube was incubated with anti-F4/80 Ab-PE, anti-CD45 Ab-PerCP-Cy5.5 (BD Biosciences, San Jose, CA, USA) and then subjected to FACS analysis.

Primary tumor tissues were removed and cut into small pieces and digested with tissue-

dissociation solution (DMEM/F12 medium supplemented with 0.0125% Deoxyribonuclease I, 0.05% collagenase type 3, 0.0125% Neutral protease (Worthington Biochemical, Lakewood, NJ, USA) at 37°C for 30 minutes. During the incubation, the tissues were pipetted up and down every 10 minutes. Tissue-supernatants were then filtered by using a 70- μ m strainer to obtain the single-cell suspension and then were centrifuged at 1,000 rpm for 5 minutes. The supernatant was removed and cell pellet was suspended in 3 mL Red Blood Cell Lysis Solution at room temperature for 10 minutes, then was centrifuged at 1,000 rpm for 5 minutes. The cell pellet for each tumor sample was re-suspended in PBS and then separated into two tubes: one tube was incubated with anti-F4/80 Ab-PE, anti-CD45 Ab-PerCP-Cy5.5 (BD Biosciences, San Jose, CA, USA), and anti-CD3 Ab-FITC (Thermo Fisher Scientific, Waltham, MA, USA), another tube was incubated with anti-CD3 Ab-PE-Cy7 (Sungene Biotech, Tianjin, China) and anti-CD69 Ab-APC (Thermo Fisher Scientific, Waltham, MA, USA) and then subjected to FACS analysis.

To detect the presence of membrane-bound CD137 and CD137L, the RawRL, 4T1FL and M Φ were incubated with anti-CD137L Ab-FITC (Bioss Antibodies, Beijing, China), anti-CD137 Ab-FITC or IgG-FITC (Sungene Biotech, Tianjin, China) separately and then subject to FACS analysis.

Statistical analysis

t-test was used to determine the significance and data are presented as mean + standard error of the mean (SEM) unless otherwise specified. $P < 0.05$ was defined as statistically significant. In all figures, "*" indicates $P < 0.05$; "***" indicates $P < 0.01$; "ns": not significant.

Results

Elevated serum sCD137L level in patients with metastatic breast cancer

To explore the function of CD137L-CD137 signaling in the development and metastasis of breast cancer, immunohistochemistry staining of CD137 and CD137L in 36 cases of human breast cancer tissues revealed that CD137 is expressed in 25 patients (69.4%) and CD137L is expressed in 24 patients (66.7%), they are co-expressed in 18 patients (50%). In CD137 positive patients, 64% showed stromal only expression pattern and 36% showed both stromal and tumor cells expression pattern. In CD137L positive patients, 70.8% showed tumor cells only expression pattern and 29.2% showed both stromal and tumor cells expression pattern. These

results reveal that CD137 is mainly expressed in stromal sites, while CD137L is predominantly expressed in breast tumor cells (Figure 1A and Table S2), which tends to be consistent with previous reports in other types of solid tumors [12]. TCGA database analysis showed that CD137 and CD137L correlated with the macrophage markers, such as CD14, CD33, and CD68 at the mRNA level, respectively (Figure S1A). In addition, CD137 mRNA correlated with CD137L mRNA in these breast cancer tissues (Figure S1B). To test the association of monocytes/macrophages with metastases of breast cancer clinically, serum soluble CD68 (sCD68) in age-matched normal female, female breast cancer patients with or without metastasis was measured (patient information was summarized in Table S3). The expression level of sCD68 in serum of metastatic breast cancer patients was significantly higher than that of the other two groups (Figure 1B). Consistently, significantly higher level of soluble CD137L (sCD137L) in the serum of patients with metastatic breast cancer was also found than in that of normal and non-metastatic groups (Figure 1C, patient information was summarized in Table S4). Based on these observations, we speculate that CD137L-CD137

signaling may be associated with metastases of breast cancer.

CD137 enhances the migration of monocytes/macrophages and promotes their differentiation into osteoclasts

To verify the function of CD137 in the migration of monocytes/macrophages, stable RAW264.7-Renilla luciferase cells with *Cd137* overexpression (RawRL-CD137, Figure 2A) and down-regulation (RawRL-shCD137, Figure 2B) were established. We found that CD137 promotes the expression of *Fra1*, one of the key transcriptional factors that promote cell migration and epithelial-mesenchymal transition (EMT) [39, 40]. As expected, overexpression of *Cd137* promoted the migration of monocytes/macrophages (Figure 2C and 2D, Figure S2A), while down-regulation of *Cd137* inhibited the migration (Figure 2E and S2B). In addition, RNA-seq results further showed that CD137 regulates the mRNA expression of several genes associated with cell migration (Figure 2F). Among them, 11 genes were up-regulated, and 3 genes were down-regulated in RawRL-CD137 cells as compared with RawRL-Con.

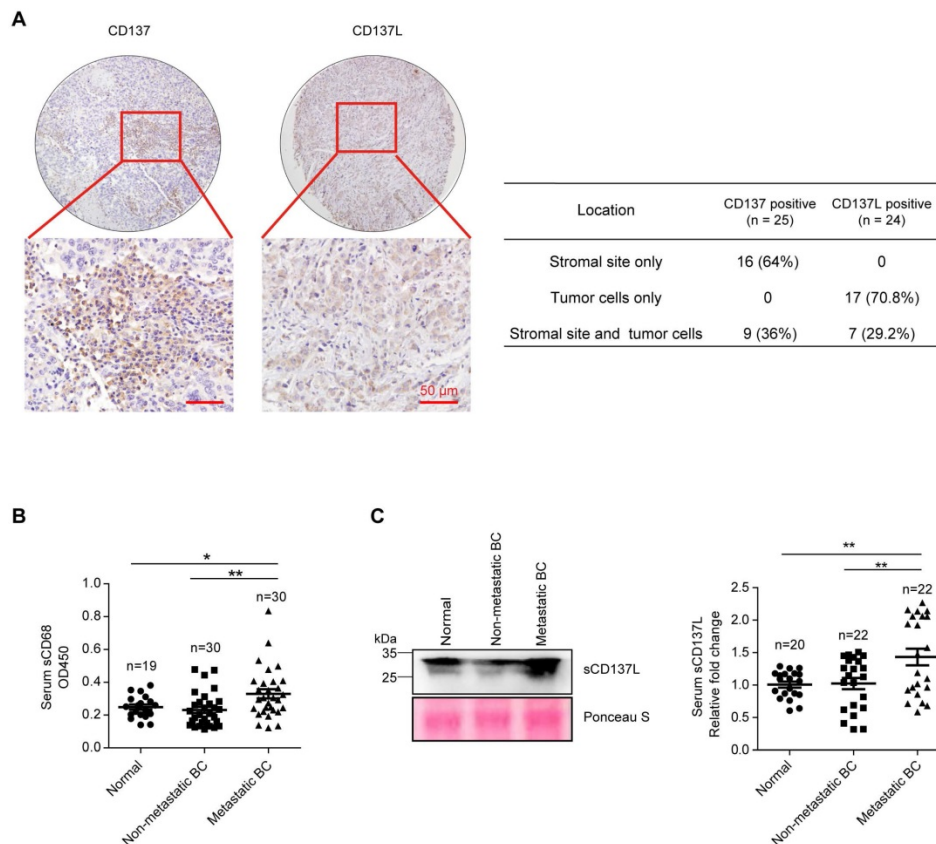


Figure 1. Elevated serum sCD137L level in patients with metastatic breast cancer. A. Representative IHC staining of CD137 and CD137L in human breast cancer tissue array (left panel, scale bar: 50 μ m) and the statistical analysis results for their expression pattern in breast tumor tissues (right panel). **B.** Statistical analysis results of OD450 value of serum sCD68 from normal female and female breast cancer (BC) patients measured by ELISA. Data are presented as mean \pm SEM. **C.** Representative Western blot results of serum sCD137L in normal female and female breast cancer (BC) patients (left panel) and the statistical analysis results of Western blot, data are presented as mean \pm SEM (right panel).

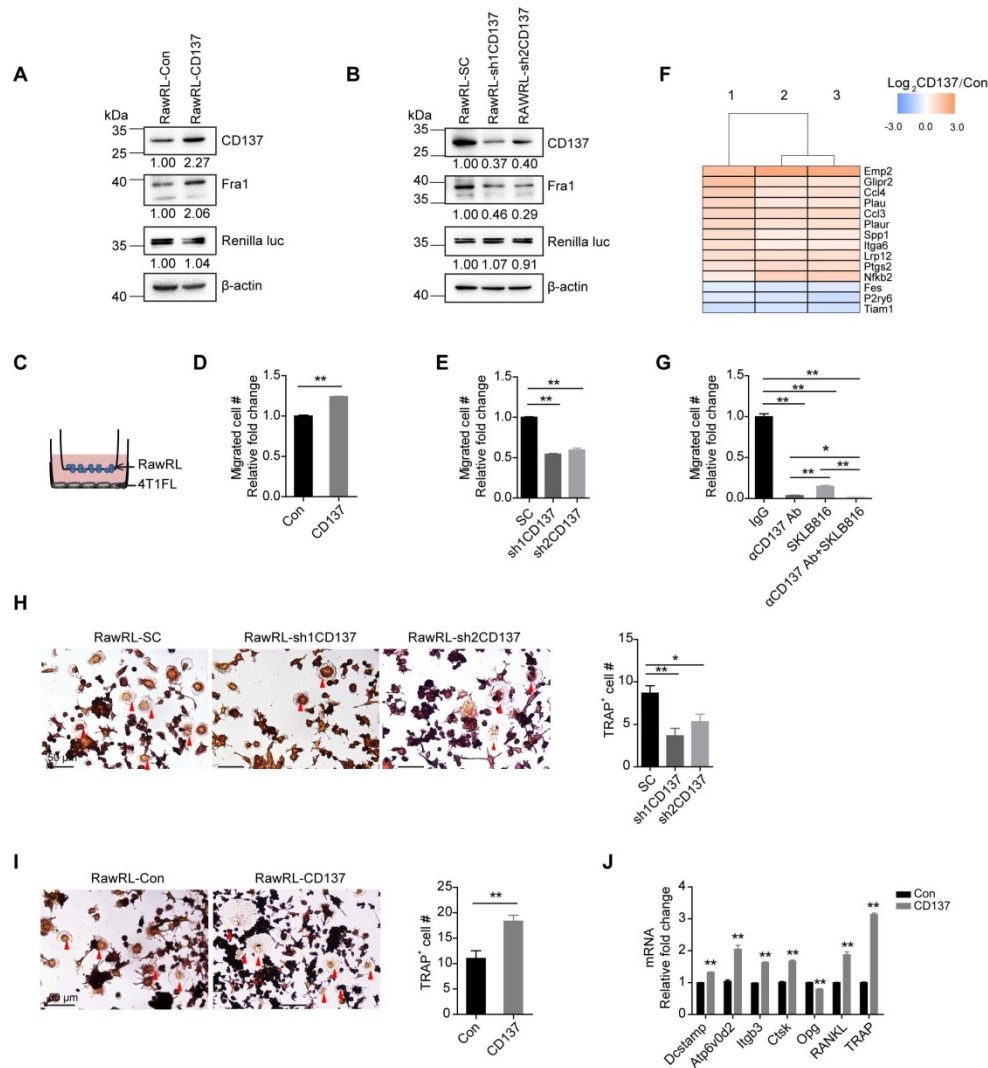


Figure 2. CD137 enhances the migration of monocytes/macrophages and promotes their differentiation into osteoclasts. A-B. Western blot results of CD137, Fra I, and renilla luciferase (Renilla luc) in RawRL cells. The mean value of relative fold change (RFC) for each blot is indicated at the bottom, n = 3. **C-E.** Schematic diagram to show the transwell assay of RawRL cells (C) and the statistical results for the change of migrated cell number (#) per image field from the transwell assay (D-E, n = 3). **F.** RNA-seq results for the differential expression genes associated with cell migration in RawRL-CD137 cells when compared with RawRL-Con. **G.** Statistical results for the change of migrated cell number per image field from the transwell assay of RawRL-CD137 cells that treated with α CD137 Ab, SKLB816 (Fra I inhibitor) and the combination of α CD137 Ab and SKLB816, respectively. IgG treatment was used as the control, (n = 3). **H-I.** TRAP staining of RawRL cells which were treated with M-CSF (10 ng/mL) and RANKL (100 ng/mL) for 9 days. Left panel: Representative image of each group, the representative osteoclasts are indicated the red arrows, scale bar: 50 μ m. Right panel: Statistical results for the number of TRAP positive osteoclasts per image field (n = 3). **J.** Real-time PCR assay of relative mRNA level change of osteoclast-related genes in RawRL cells after treatment with M-CSF (10 ng/mL) and RANKL (100 ng/mL) for 9 days (n = 3).

As shown in **Figure S2C**, overexpression of *Fra1* promoted the migration of RAW264.7 (**Figure S2C**) and rescued the inhibited migration induced by *Cd137* silencing in RawRL (**Figure S2D**). To further test the function of *Fra1* in mediating the migration-promotion effect of CD137, a *Fra1* inhibitor-SKLB816 (also named 13an) [41] was used. We found that SKLB816 can effectively reduce the expression of *Fra1* and p-*Fra1* in 4T1FL and RawRL-CD137 cells (**Figure S2E** and **S2F**). Application of anti-CD137 Ab as well as SKLB816 significantly compromised the migration of RawRL-CD137 cells (**Figure 2G**). In addition, combination of anti-CD137 Ab and SKLB816 showed higher efficacy in inhibiting the migration of

RawRL-CD137 than application of anti-CD137 Ab and SKLB816 alone (**Figure 2G**). Moreover, overexpression of *Cd137* slightly promoted the proliferation of RawRL cells (**Figure S2G**). Application of anti-CD137 Ab inhibited the proliferation of 4T1FL and RawRL-CD137 cells (**Figure S2H** and **S2I**), but did not affect the proliferation of primary cultured macrophages (M Φ , **Figure S2J**).

The expression of membrane-bound CD137 and CD137L were both detectable in RawRL, M Φ and 4T1FL cells from fluorescence-activated cell sorting (FACS) assay (**Figure S3A** and **S3B**). In addition, sCD137L was found in the supernatant of these cells

(Figure S3C). Transwell assay showed that 4T1FL cells in the lower chamber recruit more M Φ when compared with their supernatants (Figure S3D), suggesting that breast cancer cells keep secreting certain chemokines and/or cytokines to promote recruitment of monocytes/macrophages. Application of anti-CD137L blocking Ab to the lower chamber inhibited the recruitment of both RawRL and M Φ by 4T1FL cells (Figure S3D and S3E); supporting the notion that CD137L-CD137 signaling promotes the migration of monocytes/macrophages.

Previous studies showed that CD137L-CD137 signaling may regulate the differentiation of monocytes into osteoclasts by affecting the RANKL/RANK signaling pathway. The expression of membrane-bound CD137L and sCD137L increased in RawRL when they differentiated to osteoclasts (Figure S3F-S3H). Silencing of *Cd137* and application of anti-CD137L blocking Ab inhibited the differentiation of RawRL cells into osteoclasts (Figure 2H and Figure S3I). Correspondingly, overexpression of *Cd137* showed opposite effect (Figure 2I). Meanwhile, the expression of osteoclast formation and activation-related genes, such as osteoclast fusion related genes-*Dcstamp*, *Atp6v0d2*, adhesion related genes- *Itgb3*, osteoclast resorptive related genes- *Ctsk*, and the genes related to osteoclast maturation and activation- *RANKL* and *TRAP* [42] were all significantly up-regulated in RawRL-CD137 cells after stimulation with M-CSF and RANKL when compared with RawRL-Con cells (Figure 2J). Correspondingly, anti-CD137L blocking Ab inhibited the expression of *Dcstamp*, *Atp6v0d2*, *Itgb3*, *Ctsk*, *Opg* and *TRAP* in RawRL-CD137 cells after stimulation with M-CSF and RANKL (Figure S3J).

Monocyte/Macrophage expression of CD137 promotes bone metastases of breast cancer

To explore the function of monocyte/macrophage CD137 in bone metastases of breast cancer *in vivo*, we used 4T1, which is a triple-negative murine breast cancer cell line and shows high metastatic properties [43, 44], to establish 4T1 cells with firefly luciferase overexpression (4T1FL). 4T1FL cells were subcutaneously co-injected with RawRL-Con or RawRL-CD137 cells to BALB/c mice. The primary tumor was resected after two-weeks of inoculation (Figure 3A). Although there was no significant difference for the percentage of Ki67 positive cells in the primary tumors between two groups (Figure 3B), greater tumor metastatic burdens (Figure 3C) were detected by bioluminescence imaging (BLI) in mice co-injected with 4T1FL and RawRL-CD137 cells as compared with the mice co-injected with 4T1FL and RawRL-Con. The mice

were sacrificed 4 weeks after primary tumor resection and the metastatic bone specimens were collected. Bone metastases were further confirmed by H&E staining (Figure 3D). TRAP staining of bone metastatic lesions revealed an increase in the infiltration of TRAP⁺ osteoclasts in the 4T1FL plus RawRL-CD137 co-injection group as compared with the control (Figure 3E). At the same time, the percentage of RawRL cells was significantly higher in the bone metastatic lesions of 4T1FL plus RawRL-CD137 co-injection group than that of the control (Figure 3F). This finding demonstrates that overexpression of *Cd137* in RawRL promotes bone metastasis of breast tumor cells *in vivo*.

Design and preparation of a novel NP- α CD137 Ab targeting F4/80⁺ monocytes/macrophages

To further verify the role of monocytes/macrophages in bone metastases of breast cancer, we cleared the monocytes/macrophages of mice by liposome-encapsulated clodronate (clodrolip, Figure S4A). 4T1FL-allograft mouse model was established (Figure S4A). Four weeks after primary tumor resection, mice were sacrificed. Immunohistochemistry (IHC) staining of F4/80, a macrophage marker for both immune-active M1 and immune-suppressive M2 phenotype [31], in the spleens revealed that clodrolip effectively eliminated monocytes/macrophages *in vivo* (Figure S4B). BLI revealed that depletion of monocytes/macrophages significantly inhibits bone metastases of breast cancer (Figure S4C). H&E staining of bone specimens revealed that the bone metastatic burden in the clodrolip treatment group is lower than that in the PBS treatment group (Figure S4D). Meanwhile, the infiltration of TRAP⁺ osteoclasts in bone metastatic lesions of clodrolip treatment group was reduced when compared with that of PBS treatment group (Figure S4E). In addition, monocytes/macrophages depletion significantly suppressed the lung metastatic burden (Figure S4F). The above results confirm that monocytes/macrophages play an important role in promoting the metastases of breast cancer.

Based on our finding that overexpression of *Cd137* in monocytes/macrophages promoted their migration and increased bone metastases of breast cancer, we next analyzed whether blockade of their CD137 pathway could alleviate bone metastases in breast cancer. To achieve this goal, a novel F4/80 targeted liposomal nanoparticle (NP) encapsulating anti-CD137 blocking antibody (NP- α CD137 Ab-F4/80) was designed and synthesized. The procedure for preparing this NP was summarized in Figure 4A. By using the PE labelled anti-CD137 Ab, the encapsulation efficiency of NP- α CD137

Ab-PE-F4/80 was measured as ~84.76% (Figure 4B). Dynamic light scattering (DLS) measurement showed that the mean diameter of NPs- α CD137 Ab-F4/80 is ~117 nm (Figure 4C and 4D). The target efficacy of this novel NP- α CD137 Ab-PE-F4/80 was demonstrated by increased presence of α CD137

Ab-PE in the tumor tissues (Figure 4E and 4F) and the increased percentage of α CD137 Ab-PE in CD68⁺ cells when compared with the non-targeting NPs- α CD137 Ab-PE treatment group, however the percentage of CD68⁺ cells in tumor tissues was not affected (Figure 4G).

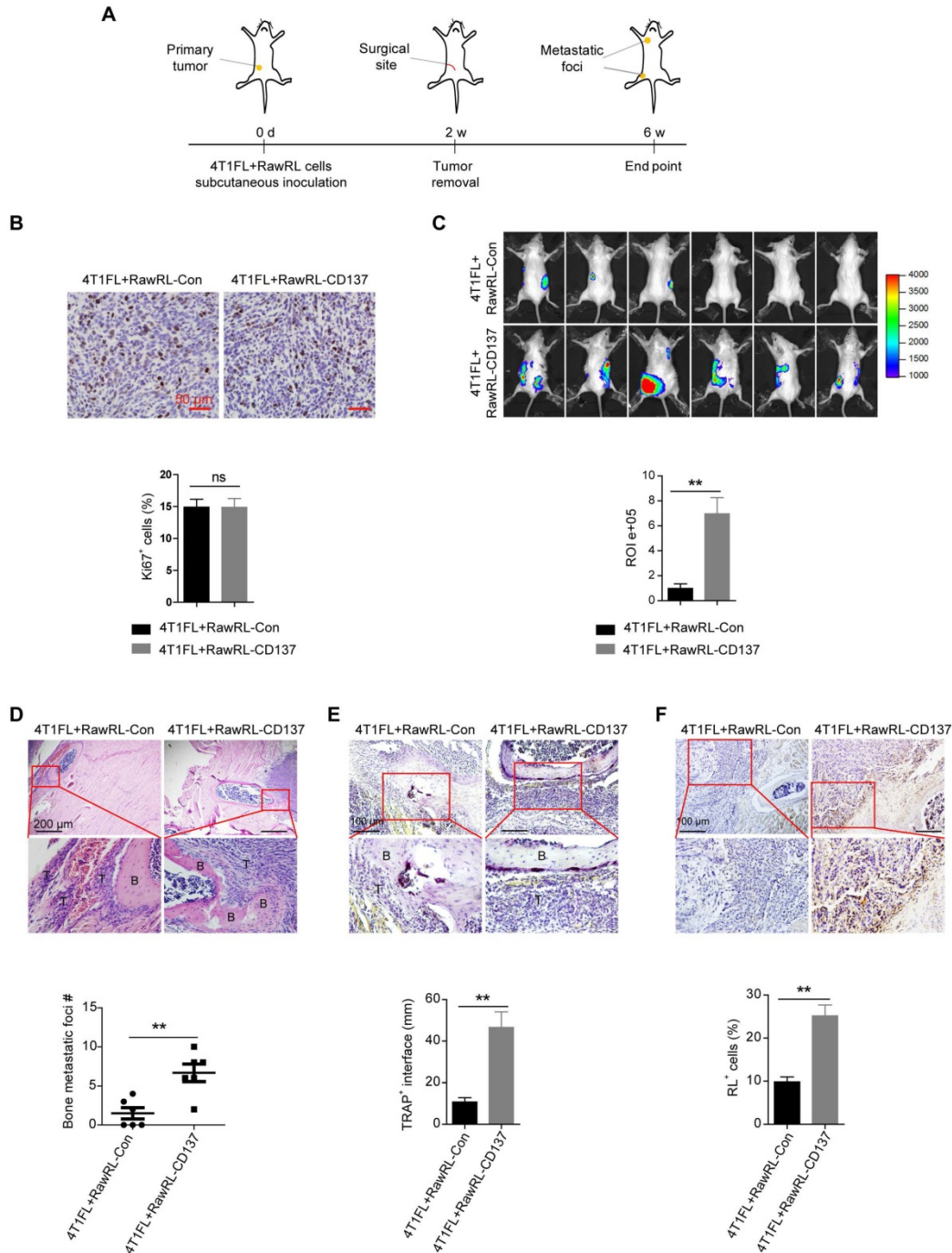


Figure 3. Monocyte/Macrophage expression of CD137 promotes bone metastases of breast cancer. **A.** Schematic diagram of experiment procedure. **B.** Representative IHC staining of Ki67 (upper panel, scale bar: 50 μ m) and the statistical results for the percentage of Ki67 positive cells in 4T1FL-allografts of BALB/c mice (lower panel, n = 5 - 6 mice). **C.** BLI images of tumor-invasion lesions in each group (upper panel) at the end point of experiment and statistical results of normalized BLI signals (lower panel, n = 6 mice). **D.** Upper panel: Representative H&E staining image of bone lesions invaded by tumors in each group, scale bar: 200 μ m. Low panel: Quantification of bone metastatic lesion number base on H&E staining, data are presented as mean \pm SEM (n = 6 mice). **E.** Upper panel: TRAP staining of the osteolytic bone lesion from a representative mouse in each group, scale bar: 100 μ m. Low panel: Statistical results of TRAP⁺ osteoclasts in osteolytic bone lesions (n = 7-11 bone lesions). **F.** Upper panel: Representative IHC staining of renilla luciferase⁺ cells in osteolytic metastasis areas, scale bar: 100 μ m. Low panel: Statistical results of the percentage of renilla luciferase (RL)⁺ cells in osteolytic bone lesions (n = 6 mice). Abbreviation: d: day(s); w: week(s); ROI: region of interest; B: bone; T: tumor.

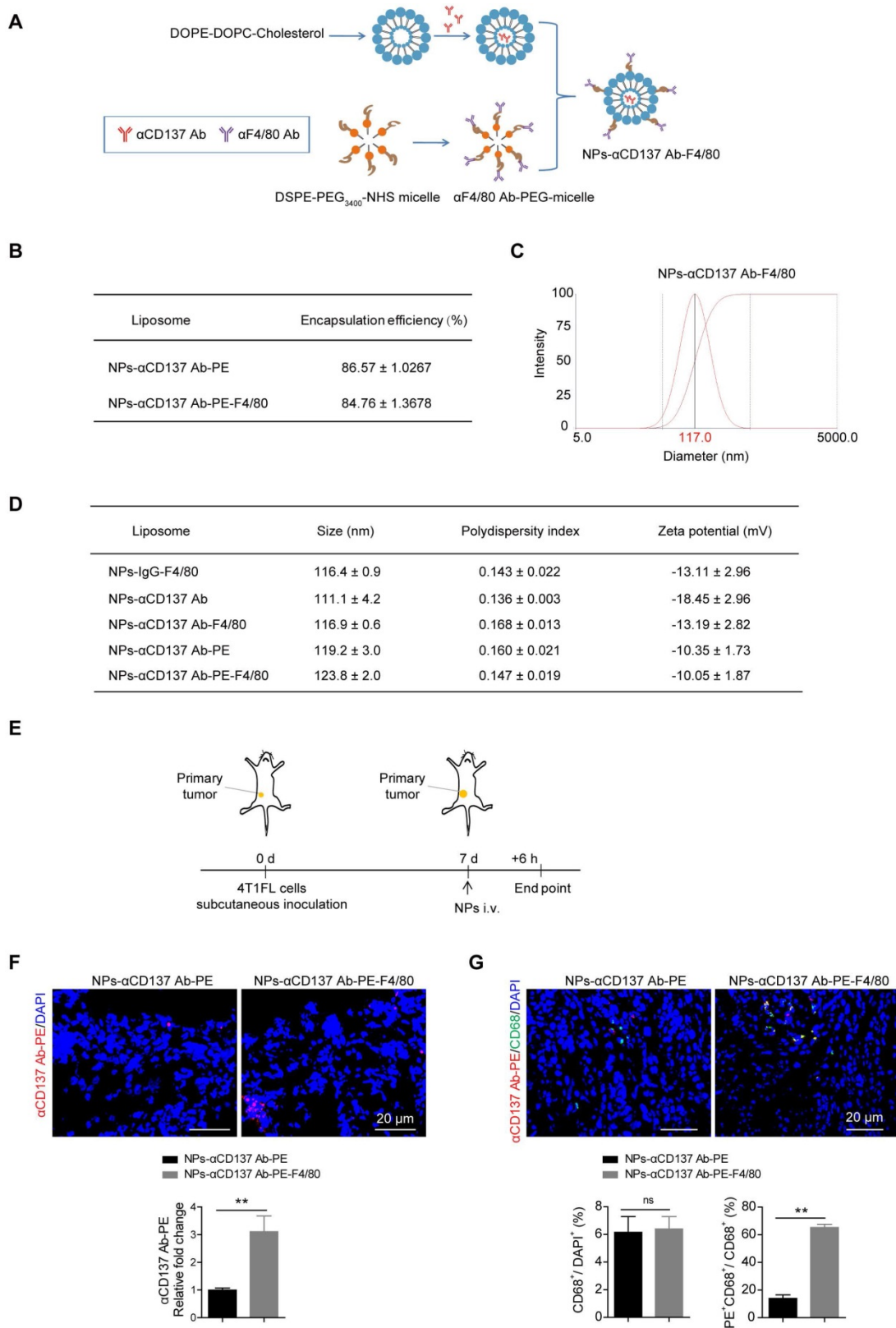


Figure 4. Increased targeting efficiency of NPs-αCD137 Ab PE-F4/80 in breast tumor tissues. **A.** Schematic diagram for the preparation of NPs-αCD137 Ab-F4/80. **B.** The encapsulation efficiency of NPs-αCD137 Ab-PE and NPs-αCD137 Ab-PE-F4/80. Data are presented as mean ± SEM (n = 3). **C.** Representative dynamic light scattering measurement for size distribution of NPs-αCD137 Ab-F4/80. **D.** The characterizations of the liposomal nanoparticles. Data are presented as mean ± SEM (n = 3). **E.** Schematic diagram of experiment procedure. **F.** Confocal images of anti-CD137 Ab-PE (upper panel, scale bar: 20 μm) and the statistical results for the relative fold changes of the concentration of anti-CD137 Ab-PE in 4T1FL-allografts of BALB/c mice that were treated with NPs-αCD137 Ab-PE or NPs-αCD137 Ab-PE-F4/80 for 6 hours (n = 4 mice, lower panel). **G.** Confocal images of anti-CD137 Ab-PE and CD68 (upper panel, scale bar: 20 μm) and the statistical results for the ratio of CD68⁺/DAPI⁺ and PE⁺CD68⁺/CD68⁺ cells in 4T1FL-allografts of BALB/c mice treated with NPs-αCD137 Ab-PE or NPs-αCD137 Ab-PE-F4/80 for 6 hours (lower panel, n = 4 mice). Abbreviation: d: day(s); i.v.: intravenous injection.

NPs- α CD137 Ab-F4/80 inhibit bone and lung metastases of breast cancer

To explore the therapeutic effect of this novel NP *in vivo*, 4T1FL-allograft mouse model was established (Figure 5A). After 1 week of 4T1FL inoculation, NPs- α CD137 Ab-F4/80 were injected via tail vein at a small dose of 6 μ g Ab/20g BW for three times, as summarized in Figure 5A. We found that NPs- α CD137 Ab-F4/80 significantly inhibit bone metastases of breast cancer when compared to the PBS, α CD137 Ab, NPs- α CD137 Ab treatment groups (Figure 5B). H&E staining revealed that bone metastatic burden in the NPs- α CD137 Ab-F4/80 treatment group is lower than that in the controls (PBS, NPs-IgG-F4/80, α CD137 Ab, NPs- α CD137 Ab treatment group, Figure 5C). Meanwhile, TRAP staining showed that the infiltration of TRAP-positive osteoclasts in bone metastatic lesions of NPs- α CD137 Ab-F4/80 treatment group was significantly lower than that of controls (Figure 5D). In addition, NPs- α CD137 Ab-F4/80 decreased the lung metastatic burden of breast cancer (Figure 5E). At the same time, the weight of mice in NPs- α CD137 Ab-F4/80 treatment group did not obviously change when compared with the other groups (Figure 5F).

Although NPs- α CD137 Ab-F4/80 treatment increased the monocytes in peripheral blood, the mean number of monocytes remained within the normal range (< 9 % of white blood cells). It has no effect on the number of other peripheral blood cells (Figure S6A and S6B) and percentage of monocytes/macrophages (CD45^{high}F4/80^{high}, CD45^{hi}F4/80^{hi} cells) in the spleen (Figure S6C and S6D). Since CD137 has been well recognized as a costimulatory molecule for T-cell activation, we tested whether the NPs affect the activation of T cells. The markers for T cell activation- CD44 and CD69 [45, 46] were detected in mouse spleens by FACS. We found that the percentage of CD3^{hi} cells, and the ratios of CD69^{hi}CD4^{hi}/CD3^{hi}, CD69^{hi}CD8^{hi}/CD3^{hi}, CD44^{hi}CD4^{hi}/CD3^{hi}, CD44^{hi}CD8^{hi}/CD3^{hi} cells in spleen leukocytes were not obviously affected upon NPs- α CD137 Ab-F4/80 treatment as compared with the PBS treatment control (Figure S6E-S6F). At the same time, the percentages of CD45^{hi}CD3^{hi} and CD3^{hi}CD69^{hi} cells in tumor tissues did not significantly change after the NPs- α CD137 Ab-F4/80 treatment (Figure S6G-S6J), indicating that NPs- α CD137 Ab-F4/80 treatment has no influence on the presence and activation of T cells in tumor tissues. These findings were further verified by the immunofluorescent staining of CD3 and CD69 in tumor tissues (Figure S6K and S6L). In addition, the

percentage of CD45^{hi}F4/80^{hi} cells and the ratio of CD68⁺/DAPI⁺ cells in tumor allografts did not change upon NPs- α CD137 Ab-F4/80 treatment (Figure S6G and S6H, Figure S6K and S6L), but the ratio of Ki67⁺/DAPI⁺ cells reduced (Figure S6K and S6L), demonstrating that the NPs- α CD137 Ab-F4/80 inhibit the proliferation of primary tumor but do not affect the presence of macrophages in tumor microenvironment.

Dual-target therapy for breast cancer against CD137 and Fra1

Since we demonstrated that CD137 promotes the expression of Fra1, we asked whether our synthesized nanoparticles could increase the anti-metastasis efficacy of the Fra1 inhibitor *in vivo*. To test this hypothesis, 4T1FL-allograft mouse model was established. NPs- α CD137 Ab-F4/80 were injected via the tail vein for a total of three doses, SKLB816 was injected for a total of six doses as summarized in Figure 6A. Mice treated with PBS, NPs- α CD137 Ab-F4/80 or SKLB816 only at the same dose and frequency were used as controls. We found that SKLB816 reduces bone metastatic burden when compared with the PBS treatment group (Figure 6B). The bone metastatic burden was also decreased in the combined treatment mice when compared with the PBS treatment group. Meanwhile, the combined therapy reduced both the lung metastatic foci number and area ratio in the 4TFL-bearing mice when compared with the PBS, NPs- α CD137 Ab-F4/80 or SKLB816 treatment alone group separately (Figure 6C). The above findings demonstrated that NPs- α CD137 Ab-F4/80 can intensify the therapeutic efficacy of the SKLB816 *in vivo* and thus provide a potential new combined therapeutic strategy for the treatment of distant metastases of breast cancer.

Schematic summary of our proposed model is shown in Figure 6D. Specifically, Fra1 was reported to be activated by MEK-ERK/JNK signaling in monocytes/macrophages [47]. Here, we found that CD137 signaling promotes the expression of Fra1, although the underlying regulatory mechanisms still need to be explored. The NPs- α CD137 Ab-F4/80 block the CD137 signaling of macrophages in tumor microenvironment, which on the one hand inhibit the differentiation of macrophage into osteoclasts, and on the other hand inhibit the expression of Fra1 to reduce the migration property of macrophages. Moreover, the NPs- α CD137 Ab-F4/80 increases the anti-metastatic effect of SKLB816, which inhibits the expression of Fra1 in both macrophages and tumor cells.

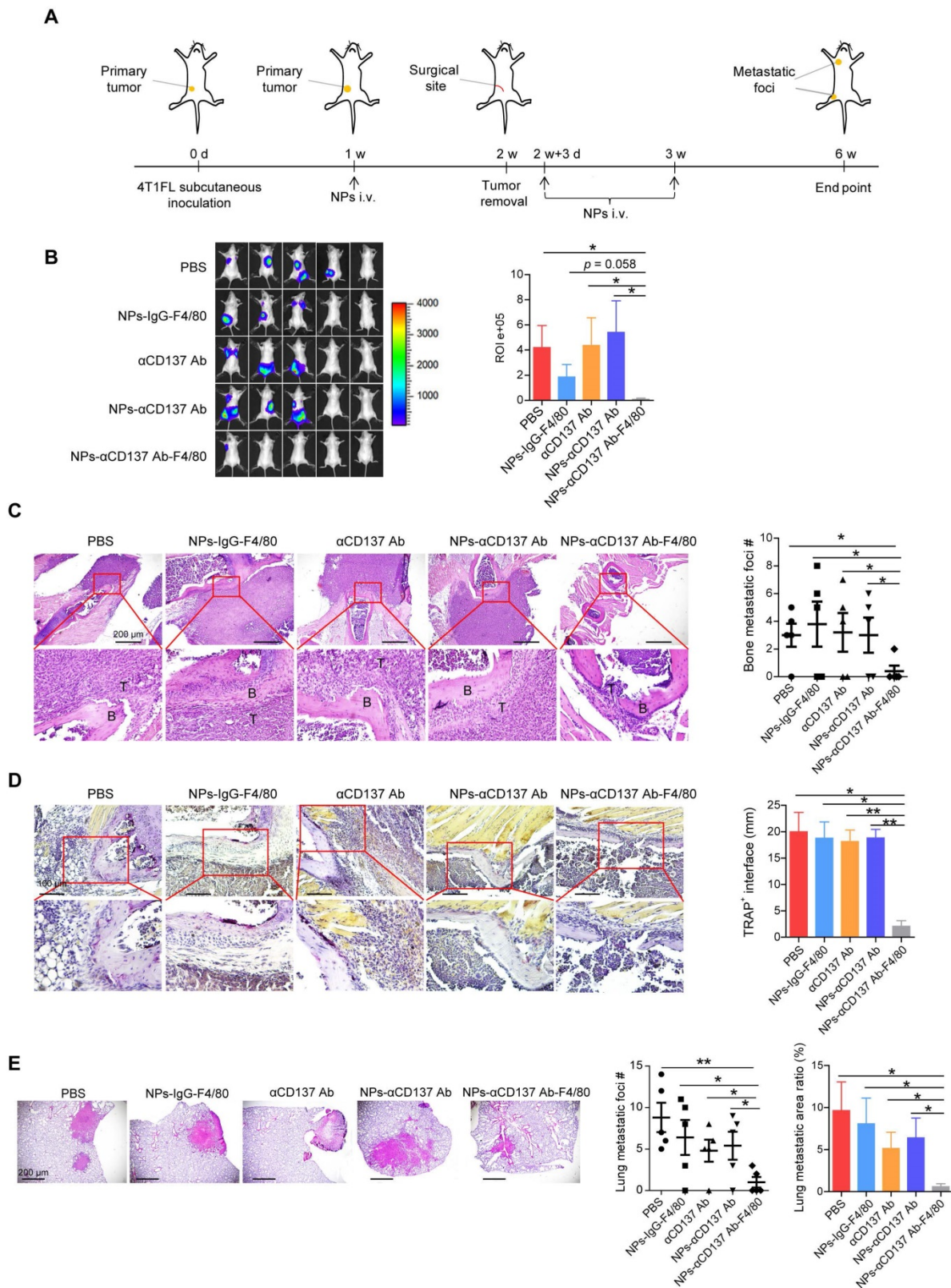


Figure 5. NPs-αCD137 Ab-F4/80 inhibit bone and lung metastases of breast cancer. **A.** Schematic diagram of experiment procedure. NPs-αCD137 Ab-F4/80 and their controls (PBS, NPs-IgG-F4/80, αCD137 Ab, NPs-αCD137 Ab) were administrated at the time points indicated by arrows. **B.** Left panel: BLI images of tumor-invasion lesions in each group at the end point of experiment. Right panel: Statistical results of normalized BLI signals (n = 5 mice). **C.** Left panel: Representative H&E staining image of bone lesions invaded by tumors from each group, scale bar: 200 μm. Right panel: Statistical results of bone metastatic lesion number, data are presented as mean ± SEM (n = 5 mice). **D.** Left panel: Representative TRAP staining of the osteolytic bone lesions from each group, scale bar: 100 μm. Right panel: Statistical results of TRAP⁺ osteoclasts in osteolytic bone lesions in each group (n = 2-5 bone lesions). **E.** Left panel: H&E staining of lung metastasis from a representative mouse in each group, scale bar: 200 μm. Right panel: Statistical results of lung metastatic foci number (data are presented as mean ± SEM) and lung metastatic area ratio in each group (n = 5 mice). Abbreviation: d: day(s); w: week(s); i.v.: intravenous injection.

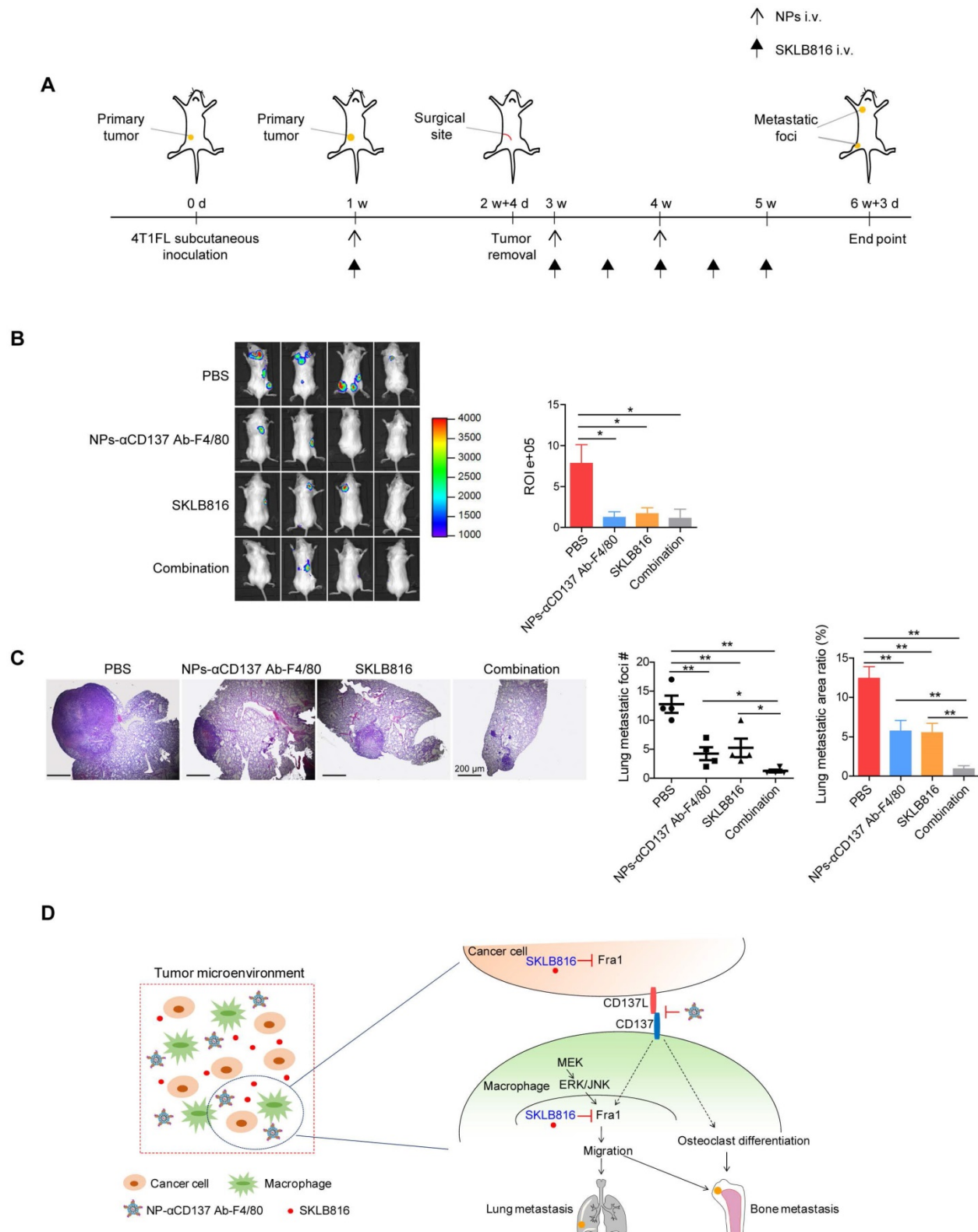


Figure 6. Dual-target therapy against CD137 and Fra1 for breast cancer. A. Schematic diagram of experiment procedure. Combined therapy (NPs-αCD137 Ab-F4/80 plus SKLB816) and the controls (PBS, NPs-αCD137 Ab-F4/80, SKLB816) were administrated at time points indicated by the corresponding arrows. **B.** Left panel: BLI images of tumor-invasion lesions in each group at the end point of experiment. Right panel: Statistical results of normalized BLI signals (n = 4 mice). **C.** Left panel: H&E staining of lung metastasis from a representative mouse in each group, scale bar: 200 μm. Right panel: Statistical results of lung metastatic foci number (data are presented as mean ± SEM) and lung metastatic area ratio (n = 4 mice). **D.** Schematic summary of our proposed model: In tumor microenvironment, NPs-αCD137 Ab-F4/80 specifically block the CD137 signaling in the macrophages, which inhibit the differentiation of macrophages into osteoclasts, and decrease the expression of Fra1 to reduce the migration property of macrophages. Moreover, the NPs increase the anti-metastatic effect of SKLB816, which inhibits the expression of Fra1 in both cancer cells and macrophages. d: day(s); w: week(s); i.v.: intravenous injection.

Discussion

Macrophages are important inflammatory cells infiltrating within most solid tumors. Their recruitment and activation in tumor microenvironment are largely regulated by signals produced by tumor, such as cytokines, chemokines, and endogenous signals, etc. [20, 48].

In this study, we demonstrated that CD137 promotes the migration of monocytes/macrophages both *in vivo* and *in vitro*, and overexpression of *Cd137* in monocytes/macrophages promotes bone metastases of breast cancer *in vivo*. Among the complex underlying mechanisms, *Fra1* was one of the import downstream factors that mediated the migration-promotion effect of CD137 in monocytes/macrophages.

Current studies showed that bone colonization of disseminated breast cancer can be detected at early stage and the osteogenic niche contributes to this procedure [49, 50]. We disclosed that the serum sCD137L level in patients with metastatic breast cancer increased when compared with breast cancer patients without metastases and normal controls. Previous study demonstrated the expression of CD137L and release of sCD137L by activated leukocytes [51]. In this study, we disclosed that besides the monocytes/macrophages, breast cancer cells also produce sCD137L. Application of anti-CD137L Ab inhibited the recruitment of monocytes/macrophages by breast cancer cells. sCD137L was considered active base on its competition with recombinant CD137L for binding to the CD137 [51]. The relative higher sCD137L in the serum of metastatic breast cancer patients may enhance the activation of CD137 signaling in monocytes/macrophages thus promote the bone and lung metastases of breast cancer cells.

Previous studies found that CD137L-CD137 bidirectional signaling pathway can enhance the differentiation of macrophages into osteoclasts [13]. However, some research groups revealed that CD137L reverse signal pathway inhibits this differentiation [52]. In our study, we found that application of anti-CD137L blocking antibody to monocytes/macrophages inhibits, but overexpression of *Cd137* promotes their differentiation into osteoclasts *in vitro*. Moreover, overexpression of *Cd137* in monocytes/macrophages increased the infiltration of TRAP⁺ osteoclasts in the bone metastatic sites of triple-negative 4T1FL breast cancer cells *in vivo*.

Current studies support the concept that advanced tumor exists in an immunosuppressive microenvironment. Blocking the immune checkpoint by anti-PD-1/PD-L1 or anti-CTLA-4 therapy shows

clinical durable responses in certain types of cancer such as renal cell carcinoma and melanoma [53-55]. However, their therapeutic efficacy on breast cancer is still under evaluation [56]. Previous studies showed that tumor associated macrophages (TAMs, M2 phenotype) are important immune suppressive cells that contribute to the growth and metastases of breast cancer [57, 58]. Targeting or reducing TAMs achieved significant therapeutic results in breast cancer [31]. In this study, depletion of F4/80⁺ monocytes/macrophages in mice with clodrolip significantly inhibited the bone-and-lung metastases of breast cancer. Targeting the F4/80⁺ macrophages to inhibit their CD137 signaling could effectively inhibit the presence of TRAP positive osteoclasts in the bone metastatic lesions of breast cancer. Our study suggests that specific blocking of CD137 signaling in monocytes/macrophage is a promising strategy in the treatment of bone metastasis of breast cancer.

In many reported immunotherapy experiments, the total dose of antibody used is usually ≥ 50 μg to reach therapeutic effects in mouse models [15, 59, 60]. In our study, low dose of antibody was loaded in the NPs (6 $\mu\text{g}/200$ uL NPs), in addition, the NPs target specifically to the macrophages/monocytes (as shown in **Figure 4**), these two key reasons may account for the inconspicuous impact of αCD137 Ab on T cell activation. This method is thus different from the anti-CD137 agonistic antibody treatment, which activates T cells and finally leads to the anti-tumor effect. Besides the two reasons above, using liposome as a carrier can reduce the ineffective degradation of loaded agents *in vivo*, thus finally enhance the therapeutic efficacy of NPs- αCD137 Ab-F4/80, which are more effective when compared with the same dose of αCD137 Ab as shown in **Figure 5**.

Previous study found that the *Fra1* inhibitor-SKLB816 has a higher therapeutic efficacy for triple-negative breast cancer when compared with other therapeutic agents such as Dasatinib and Paclitaxel [41]. Our novel NP- αCD137 Ab-F4/80 showed similar therapeutic effect in reducing the bone and lung metastasis as SKLB816 in 4T1FL-allograft mouse model. The metastasis of 4T1 is a time-dependent process. Lung is the organ where 4T1 cells are most likely to metastasize when compared with other organs such as liver, spleen, bone and brain, etc. [44]. As shown in **Figure 6**, the tumor was removed after 18 days of 4T1FL inoculation, which was relative late than the resection surgery date shown in **Figure 5** (14 days after 4T1FL inoculation), that may account for equal (100%) lung metastasis incidence observed in the NP- αCD137 Ab-F4/80 combined with the SKLB816 therapy group when compared with the control groups (PBS,

NP- α CD137 Ab-F4/80, and SKLB816 treatment groups). However, the lung metastatic foci number and area was reduced when compared with controls, indicating that the combined therapy is an effective method in reducing the lung metastasis of breast cancer.

In summary, we designed a novel F4/80 targeted liposomal nanoparticle encapsulating anti-CD137 antibody (NP- α CD137 Ab-F4/80) that could deliver the anti-CD137 antibody to monocytes/macrophages. These nanoparticles could significantly inhibit both bone and lung metastases of breast cancer. In addition, these NPs increased the anti-metastatic effects of Fra1 inhibitor on breast cancer; this study thus provided a promising strategy in the treatment of distant metastases of breast cancer.

Supplementary Material

Supplementary figures and tables.

<http://www.thno.org/v09p2950s1.pdf>

Acknowledgement

We thank Dr. Deqing Wang (Department of Blood Transfusion, Chinese PLA General Hospital, Beijing, China) for his help in blood samples collection. This work was funded by Natural Science Foundation of China 81773124, 81572599, and 81672623; Tianjin People's Hospital & Nankai University Collaborative Research Grant 2016rmnk005; Tianjin Research Program of Application Foundation and Advanced Technology 15JQJNC11700.

Competing Interests

The authors have declared that no competing interest exists.

References

- Siegel RL, Miller KD, Jemal A. Cancer statistics, 2018. *CA Cancer J Clin.* 2018; 68: 7-30.
- Sterling JA, Edwards JR, Martin TJ, Mundy GR. Advances in the biology of bone metastasis: how the skeleton affects tumor behavior. *Bone.* 2011; 48: 6-15.
- Paget S. The distribution of secondary growths in cancer of the breast. 1889. *Cancer metastasis reviews.* 1989; 8: 98-101.
- Fokas E, Engenhardt-Cabillic R, Daniilidis K, Rose F, An HX. Metastasis: the seed and soil theory gains identity. *Cancer metastasis reviews.* 2007; 26: 705-15.
- Sica G, Chen L. Biochemical and immunological characteristics of 4-1BB (CD137) receptor and ligand and potential applications in cancer therapy. *Archivum immunologiae et therapeuticae experimentalis.* 1999; 47: 275-9.
- Dharmadhikari B, Wu M, Abdullah NS, Rajendran S, Ishak ND, Nickles E, et al. CD137 and CD137L signals are main drivers of type 1, cell-mediated immune responses. *Oncoimmunology.* 2016; 5: e1113367.
- Harfuddin Z, Kwajah S, Chong Nyi Sim A, Macary PA, Schwarz H. CD137L-stimulated dendritic cells are more potent than conventional dendritic cells at eliciting cytotoxic T-cell responses. *Oncoimmunology.* 2013; 2: e26859.
- Qian Y, Pei D, Cheng T, Wu C, Pu X, Chen X, et al. CD137 ligand-mediated reverse signaling inhibits proliferation and induces apoptosis in non-small cell lung cancer. *Med Oncol.* 2015; 32: 44.
- Dimberg J, Hugander A, Wagsater D. Expression of CD137 and CD137 ligand in colorectal cancer patients. *Oncology reports.* 2006; 15: 1197-200.

- Langstein J, Michel J, Fritsche J, Kreutz M, Andreesen R, Schwarz H. CD137 (ILA/4-1BB), a member of the TNF receptor family, induces monocyte activation via bidirectional signaling. *J Immunol.* 1998; 160: 2488-94.
- Quek BZ, Lim YC, Lin JH, Tan TE, Chan J, Biswas A, et al. CD137 enhances monocyte-ICAM-1 interactions in an E-selectin-dependent manner under flow conditions. *Molecular immunology.* 2010; 47: 1839-47.
- Wang Q, Zhang P, Zhang Q, Wang X, Li J, Ma C, et al. Analysis of CD137 and CD137L expression in human primary tumor tissues. *Croatian medical journal.* 2008; 49: 192-200.
- Yang J, Park OJ, Lee YJ, Jung HM, Woo KM, Choi Y. The 4-1BB ligand and 4-1BB expressed on osteoclast precursors enhance RANKL-induced osteoclastogenesis via bi-directional signaling. *European journal of immunology.* 2008; 38: 1598-609.
- Senthilkumar R, Lee HW. CD137L- and RANKL-mediated reverse signals inhibit osteoclastogenesis and T lymphocyte proliferation. *Immunobiology.* 2009; 214: 153-61.
- Melero I, Shuford WW, Newby SA, Aruffo A, Ledbetter JA, Hellstrom KE, et al. Monoclonal antibodies against the 4-1BB T-cell activation molecule eradicate established tumors. *Nat Med.* 1997; 3: 682-5.
- Vinay DS, Kwon BS. Immunotherapy of cancer with 4-1BB. *Molecular cancer therapeutics.* 2012; 11: 1062-70.
- Tolcher AW, Sznol M, Hu-Lieskovan S, Papadopoulos KP, Patnaik A, Rasco DW, et al. Phase Ib Study of Utomilumab (PF-05082566), a 4-1BB/CD137 Agonist, in Combination with Pembrolizumab (MK-3475) in Patients with Advanced Solid Tumors. *Clin Cancer Res.* 2017; 23: 5349-57.
- Segal NH, Logan TF, Hodi FS, McDermott D, Melero I, Hamid O, et al. Results from an Integrated Safety Analysis of Urelumab, an Agonist Anti-CD137 Monoclonal Antibody. *Clin Cancer Res.* 2017; 23: 1929-36.
- Soki FN, Cho SW, Kim YW, Jones JD, Park SI, Koh AJ, et al. Bone marrow macrophages support prostate cancer growth in bone. *Oncotarget.* 2015; 6: 35782-96.
- Chittezhath M, Dhillon MK, Lim JY, Laoui D, Shalova IN, Teo YL, et al. Molecular profiling reveals a tumor-promoting phenotype of monocytes and macrophages in human cancer progression. *Immunity.* 2014; 41: 815-29.
- Vasiliadou I, Hohen I. The role of macrophages in bone metastasis. *Journal of bone oncology.* 2013; 2: 158-66.
- Kaur S, Raggatt LJ, Batoon L, Hume DA, Levesque JP, Pettit AR. Role of bone marrow macrophages in controlling homeostasis and repair in bone and bone marrow niches. *Seminars in cell & developmental biology.* 2017; 61: 12-21.
- Panni RZ, Linehan DC, DeNardo DG. Targeting tumor-infiltrating macrophages to combat cancer. *Immunotherapy.* 2013; 5: 1075-87.
- Pyonteck SM, Gadea BB, Wang HW, Gocheva V, Hunter KE, Tang LH, et al. Deficiency of the macrophage growth factor CSF-1 disrupts pancreatic neuroendocrine tumor development. *Oncogene.* 2012; 31: 1459-67.
- Hung JY, Horn D, Woodruff K, Prihoda T, LeSaux C, Peters J, et al. Colony-stimulating factor 1 potentiates lung cancer bone metastasis. *Lab Invest.* 2014; 94: 371-81.
- Mizutani K, Sud S, McGregor NA, Martinovski G, Rice BT, Craig MJ, et al. The chemokine CCL2 increases prostate tumor growth and bone metastasis through macrophage and osteoclast recruitment. *Neoplasia.* 2009; 11: 1235-42.
- Hiraoka K, Zenmyo M, Watari K, Iguchi H, Fotovati A, Kimura YN, et al. Inhibition of bone and muscle metastases of lung cancer cells by a decrease in the number of monocytes/macrophages. *Cancer science.* 2008; 99: 1595-602.
- Austyn JM, Gordon S. F4/80, a monoclonal antibody directed specifically against the mouse macrophage. *European journal of immunology.* 1981; 11: 805-15.
- Chang MK, Raggatt LJ, Alexander KA, Kuliwaba JS, Fazzalari NL, Schroder K, et al. Osteal tissue macrophages are intercalated throughout human and mouse bone lining tissues and regulate osteoblast function in vitro and in vivo. *J Immunol.* 2008; 181: 1232-44.
- Barros MH, Hauck F, Dreyer JH, Kempkes B, Niedobitek G. Macrophage polarisation: an immunohistochemical approach for identifying M1 and M2 macrophages. *PLoS One.* 2013; 8: e80908.
- Luo Y, Zhou H, Krueger J, Kaplan C, Lee SH, Dolman C, et al. Targeting tumor-associated macrophages as a novel strategy against breast cancer. *The Journal of clinical investigation.* 2006; 116: 2132-41.
- Etzerodt A, Maniecki MB, Graversen JH, Moller HJ, Torchilin VP, Moestrup SK. Efficient intracellular drug-targeting of macrophages using stealth liposomes directed to the hemoglobin scavenger receptor CD163. *Journal of controlled release : official journal of the Controlled Release Society.* 2012; 160: 72-80.
- Bertrand N, Wu J, Xu X, Kamaly N, Farokhzad OC. Cancer nanotechnology: the impact of passive and active targeting in the era of modern cancer biology. *Advanced drug delivery reviews.* 2014; 66: 2-25.
- Hamad I, Moghimi SM. Critical issues in site-specific targeting of solid tumours: the carrier, the tumour barriers and the bioavailable drug. *Expert opinion on drug delivery.* 2008; 5: 205-19.
- Guo C, Chen Y, Gao W, Chang A, Ye Y, Shen W, et al. Liposomal Nanoparticles Carrying anti-IL6R Antibody to the Tumour Microenvironment Inhibit Metastasis in Two Molecular Subtypes of Breast Cancer Mouse Models. *Theranostics.* 2017; 7: 775-88.
- Chen S, Xu Y, Chen Y, Li X, Mou W, Wang L, et al. SOX2 Gene Regulates the Transcriptional Network of Oncogenes and Affects Tumorigenesis of Human Lung Cancer Cells. *PLoS One.* 2012; 7: e36326.

37. Chen S, Li X, Lu D, Xu Y, Mou W, Wang L, et al. SOX2 regulates apoptosis through MAP4K4-Survivin signaling pathway in human lung cancer cells. *Carcinogenesis*. 2014; 35: 613-23.
38. Hu S, Dong X, Gao W, Stupack D, Liu Y, Xiang R, et al. Alternative promotion and suppression of metastasis by JNK2 governed by its phosphorylation. *Oncotarget*. 2017; 8: 56569-81.
39. Renaud SJ, Kubota K, Rumi MA, Soares MJ. The FOS transcription factor family differentially controls trophoblast migration and invasion. *J Biol Chem*. 2014; 289: 5025-39.
40. Tam WL, Lu H, Buikhuisen J, Soh BS, Lim E, Reinhardt F, et al. Protein kinase C alpha is a central signaling node and therapeutic target for breast cancer stem cells. *Cancer cell*. 2013; 24: 347-64.
41. Zhang CH, Chen K, Jiao Y, Li LL, Li YP, Zhang RJ, et al. From Lead to Drug Candidate: Optimization of 3-(Phenylethynyl)-1H-pyrazolo[3,4-d]pyrimidin-4-amine Derivatives as Agents for the Treatment of Triple Negative Breast Cancer. *Journal of medicinal chemistry*. 2016; 59: 9788-805.
42. Boyce BF. Advances in the regulation of osteoclasts and osteoclast functions. *J Dent Res*. 2013; 92: 860-7.
43. Kaur P, Nagaraja GM, Zheng H, Gizachew D, Galukande M, Krishnan S, et al. A mouse model for triple-negative breast cancer tumor-initiating cells (TNBC-TICs) exhibits similar aggressive phenotype to the human disease. *BMC Cancer*. 2012; 12: 120.
44. Tao K, Fang M, Alroy J, Sahagian GG. Imagable 4T1 model for the study of late stage breast cancer. *BMC Cancer*. 2008; 8: 228.
45. Huet S, Groux H, Caillou B, Valentin H, Prieur AM, Bernard A. CD44 contributes to T cell activation. *J Immunol*. 1989; 143: 798-801.
46. Ziegler SF, Ramsdell F, Alderson MR. The activation antigen CD69. *Stem Cells*. 1994; 12: 456-65.
47. Wagner EF, Matsuo K. Signalling in osteoclasts and the role of Fos/AP1 proteins. *Annals of the rheumatic diseases*. 2003; 62 Suppl 2: ii83-5.
48. Mantovani A, Allavena P, Sica A, Balkwill F. Cancer-related inflammation. *Nature*. 2008; 454: 436-44.
49. Hosseini H, Obradovic MM, Hoffmann M, Harper KL, Sosa MS, Werner-Klein M, et al. Early dissemination seeds metastasis in breast cancer. *Nature*. 2016.
50. Wang H, Yu C, Gao X, Welte T, Muscarella AM, Tian L, et al. The osteogenic niche promotes early-stage bone colonization of disseminated breast cancer cells. *Cancer cell*. 2015; 27: 193-210.
51. Salih HR, Schmetzer HM, Burke C, Starling GC, Dunn R, Pelka-Fleischer R, et al. Soluble CD137 (4-1BB) ligand is released following leukocyte activation and is found in sera of patients with hematological malignancies. *J Immunol*. 2001; 167: 4059-66.
52. Saito K, Ohara N, Hotokezaka H, Fukumoto S, Yuasa K, Naito M, et al. Infection-induced up-regulation of the costimulatory molecule 4-1BB in osteoblastic cells and its inhibitory effect on M-CSF/RANKL-induced in vitro osteoclastogenesis. *J Biol Chem*. 2004; 279: 13555-63.
53. Massari F, Santoni M, Ciccarese C, Santini D, Alfieri S, Martignoni G, et al. PD-1 blockade therapy in renal cell carcinoma: current studies and future promises. *Cancer treatment reviews*. 2015; 41: 114-21.
54. Ribeiro Gomes J, Schmerling RA, Haddad CK, Racy DJ, Ferrigno R, Gil E, et al. Analysis of the Abscopal Effect With Anti-PD1 Therapy in Patients With Metastatic Solid Tumors. *Journal of immunotherapy*. 2016; 39: 367-72.
55. Wolchok JD, Chan TA. Cancer: Antitumour immunity gets a boost. *Nature*. 2014; 515: 496-8.
56. Solinas C, Gombos A, Latifyan S, Piccart-Gebhart M, Kok M, Buisseret L. Targeting immune checkpoints in breast cancer: an update of early results. *ESMO open*. 2017; 2: e000255.
57. Mou W, Xu Y, Ye Y, Chen S, Li X, Gong K, et al. Expression of Sox2 in breast cancer cells promotes the recruitment of M2 macrophages to tumor microenvironment. *Cancer Lett*. 2015; 358: 115-23.
58. Yang J, Liao D, Chen C, Liu Y, Chuang TH, Xiang R, et al. Tumor-associated macrophages regulate murine breast cancer stem cells through a novel paracrine EGFR/Stat3/Sox-2 signaling pathway. *Stem Cells*. 2013; 31: 248-58.
59. Dahan R, Barnhart BC, Li F, Yamniuk AP, Korman AJ, Ravetch JV. Therapeutic Activity of Agonistic, Human Anti-CD40 Monoclonal Antibodies Requires Selective FcγR Engagement. *Cancer cell*. 2016; 29: 820-31.
60. Cheng H, Clarkson PW, Gao D, Pacheco M, Wang Y, Nielsen TO. Therapeutic Antibodies Targeting CSF1 Impede Macrophage Recruitment in a Xenograft Model of Tenosynovial Giant Cell Tumor. *Sarcoma*. 2010; 2010: 174528.